

Phenomenology of Charm and Bottom Production*

R. Vogt[†]

Nuclear Science Division, Lawrence Berkeley Laboratory, Berkeley, CA 94720, USA

and

Physics Department, University of California at Davis, Davis, CA 95616 USA

Abstract

We discuss the renormalization and factorization scale dependence of charm and bottom production both at fixed-target energies and at present and future colliders. We investigate whether distributions calculable at leading order can be extrapolated to next-to-leading order by a constant multiplicative factor.

* This work was supported in part by the Director, Office of Energy Research, Division of Nuclear Physics of the Office of High Energy and Nuclear Physics of the U. S. Department of Energy under Contract Number DE-AC03-76SF0098.

[†] For detailed numerical results, contact vogt@nsdssd.lbl.gov.

Heavy quark hadroproduction is currently being studied both at fixed-target energies with proton and pion beams and at collider energies. Additionally, charm and bottom quark production will be copious at the future RHIC and LHC colliders where nucleus-nucleus collisions are expected to produce a deconfined state of quarks and gluons, the quark-gluon plasma. Signatures of deconfinement include lepton pair production by partons in the plasma [1] and an enhancement of heavy quark production [2,3]. Thus a detailed knowledge of heavy quark production is required to separate its production during the initial nucleon-nucleon collisions from that by the quark-gluon plasma.

Previous measurements of the $c\bar{c}$ production cross section at $\sqrt{S} \leq 63$ GeV suggested that the lowest order (Born) cross section underpredicted the data by a factor of two to three [4,5], called the K factor after a similar situation in Drell-Yan production. More generally,

$$K_{\text{exp}} = \frac{\sigma_{\text{data}}(AB \rightarrow Q\bar{Q})}{\sigma_{\text{theory}}(AB \rightarrow Q\bar{Q})}, \quad (1)$$

where Q is the produced heavy quark. The projectile and target, A and B , can be either hadrons or nuclei. The next-to-leading order (NLO) corrections to the Born cross section have been calculated [6–8] and an analogous theoretical K factor can be defined from the ratio of the NLO to the Born cross sections,

$$K_{\text{th}} = \frac{\sigma_{\text{NLO}}(AB \rightarrow Q\bar{Q})}{\sigma_{\text{Born}}(AB \rightarrow Q\bar{Q})}, \quad (2)$$

where σ_{NLO} is the sum of the Born and $\mathcal{O}(\alpha_s)$ corrections. Particularly for the “lighter” heavy quarks, c and b , the NLO cross section is strongly dependent on the choice of the renormalization and factorization scales which determine both K_{exp} and K_{th} .

In this paper we discuss the scale dependence of c and b quark production and its influence on the K factors. While we explore the dependence within the limits of perturbative QCD, we adjust the scales and the heavy quark mass, m_Q , to achieve $K_{\text{exp}}^{\text{NLO}} \approx 1^1$ [9] keeping in mind that further corrections to the cross section could also be large. We use these mass

¹ $K_{\text{exp}}^{\text{NLO}}$ is the K factor for the data compared to the NLO theory calculation.

and scale parameters to predict the cross sections and K_{th} for charm and bottom production at RHIC and LHC energies, $\sqrt{S} = 200\text{-}500$ GeV and $5.5\text{-}14$ TeV respectively. Since only the Born contribution is often used in event generators, it is important to check that the distributions calculable at the Born level are a good approximation to the NLO results. We show that K_{th} is nearly constant if the renormalization and factorization scales are assumed to be a function of the heavy quark transverse momentum, p_T . Our calculations are done with a Monte Carlo program developed by Nason and collaborators [6,7,10].

The double differential cross section for $Q\bar{Q}$ pair production by hadrons A and B is

$$E_Q E_{\bar{Q}} \frac{d\sigma_{AB}}{d^3p_Q d^3p_{\bar{Q}}} = \sum_{i,j} \int dx_1 dx_2 F_i^A(x_1, \mu_F) F_j^B(x_2, \mu_F) E_Q E_{\bar{Q}} \frac{d\hat{\sigma}_{ij}(x_1 P_1, x_2 P_2, m_Q, \mu_F, \mu_R)}{d^3p_Q d^3p_{\bar{Q}}} . \quad (3)$$

Here i and j are the interacting partons and the functions F_i are the number densities of gluons, light quarks and antiquarks ($m < m_Q$) evaluated at momentum fraction x and factorization scale μ_F . The short-distance cross section, $\hat{\sigma}_{ij}$, is calculable as a perturbation series in $\alpha_s(\mu_R)$ where the strong coupling constant is evaluated at the renormalization scale μ_R . Both μ_F and μ_R are of the order of the heavy quark mass.

At the Born level, $\mathcal{O}(\alpha_s^2)$, the cross section can be written as

$$E_Q E_{\bar{Q}} \frac{d\sigma_{AB}}{d^3p_Q d^3p_{\bar{Q}}} = \int \frac{s}{2\pi} dx_1 dx_2 C(x_1, x_2) \delta^4(x_1 P_1 + x_2 P_2 - p_Q - p_{\bar{Q}}) \quad (4)$$

where \sqrt{s} , the parton-parton center-of-mass energy, is related to \sqrt{S} , the hadron-hadron center-of-mass energy, by $s = x_1 x_2 S \geq 4m_Q^2$. The intrinsic transverse momenta of the incoming partons have been neglected. The convolution of the subprocess cross sections with the parton number densities is contained in $C(x_1, x_2)$,

$$C(x_1, x_2) = \sum_q [F_q^A(x_1) F_{\bar{q}}^B(x_2) + F_{\bar{q}}^A(x_1) F_q^B(x_2)] \frac{d\hat{\sigma}_{q\bar{q}}}{dt} + F_g^A(x_1) F_g^B(x_2) \frac{d\hat{\sigma}_{gg}}{dt} , \quad (5)$$

where production is by $q\bar{q}$ annihilation, $q\bar{q} \rightarrow Q\bar{Q}$, and gluon fusion, $gg \rightarrow Q\bar{Q}$. The scale dependence has been suppressed since there is no distinction between μ_F and μ_R at this order. The scale $2m_Q$ is commonly used for the total cross section, motivated by the s -channel processes. However, the t and u channel gluon fusion graphs involve heavy quark

exchange between the gluons, suggesting that m_Q is a better scale choice. Thus some ambiguity in scale already exists at leading order.

Four-momentum conservation leads to the rather simple expression

$$\frac{d\sigma_{AB}}{dp_T^2 dy_Q dy_{\bar{Q}}} = x_1 x_2 C(x_1, x_2) , \quad (6)$$

where the momentum fractions, x_1 and x_2 , are

$$x_{1,2} = \frac{m_T}{\sqrt{s}} (e^{\pm y_Q} + e^{\pm y_{\bar{Q}}}) , \quad (7)$$

and $m_T = \sqrt{m_Q^2 + p_T^2}$. The target fraction, x_2 , decreases with rapidity while the projectile fraction, x_1 , increases. Both increase with p_T . The quark p_T distribution is determined by $d\hat{\sigma}_{ij}/dt \propto 1/m_T^4$, as discussed in [11].

At NLO, $\mathcal{O}(\alpha_s^3)$, in addition to real and virtual corrections to the Born diagrams, quark-gluon scattering, $q(\bar{q})g \rightarrow Q\bar{Q}q(\bar{q})$, is also included. At the Born level, this has been interpreted as scattering a heavy quark in the hadron sea with a light quark or gluon and referred to as flavor excitation² [11]. The relative importance of the excitation diagrams to hadroproduction is shown in Ref. [13].

The total short-distance cross section, $\hat{\sigma}_{ij}$, is

$$\hat{\sigma}_{ij}(s, m_Q, \mu_F, \mu_R) = \frac{\alpha_s^2(\mu_R)}{m_Q^2} \left\{ f_{ij}^0(\rho) + 4\pi\alpha_s(\mu_R) \left[f_{ij}^1(\rho) + \bar{f}_{ij}^1(\rho) \ln(\mu_F^2/m_Q^2) \right] + \mathcal{O}(\alpha_s^2) \right\} , \quad (8)$$

where $\rho = 4m_Q^2/s$ and the functions f_{ij}^n are coefficients of the perturbative expansion. The Born contribution is given by f_{ij}^0 and vanishes when $ij = gq, g\bar{q}$. The Born coefficients are always positive and $f_{ij}^0 \rightarrow 0$ as $\rho \rightarrow 0$. The NLO coefficients can be either positive or negative and tend to finite values as $\rho \rightarrow 0$ in the gg and $q\bar{q}$ channels. The mass factorization terms, \bar{f}_{ij}^1 , only contribute when $\mu_R \neq m_Q$. The gg and qg contributions are dominant in the high energy limit due to t -channel gluon exchange. The NLO gg corrections are very

²In deep-inelastic scattering when $Q^2 \gg m_Q^2$ the heavy quark can be treated as massless and absorbed into the parton densities but when $Q^2 \sim m_Q^2$, flavor creation diagrams are dominant [12].

large since $f_{gg}^1/f_{gg}^0 \rightarrow \infty$ as $\rho \rightarrow 0$, indicating that a small x resummation is needed. For completeness, in Fig. 1, the coefficients are reproduced from Ref. [6] as a function of $1/\sqrt{\rho} = \sqrt{s}/2m_Q$. Although the coefficients are shown for $1/\sqrt{\rho} < 200$ only, f_{ij}^1 and \bar{f}_{ij}^1 have reached a plateau. The maximum value of $1/\sqrt{\rho}$ for a given energy is $1/\sqrt{\rho_{\max}} = \sqrt{S}/2m_Q$, so that $3 \leq 1/\sqrt{\rho_{\max}} \leq 12$ at typical fixed-target energies while $1/\sqrt{\rho_{\max}} > 20$ for $b\bar{b}$ production and > 77 for $c\bar{c}$ production at RHIC and LHC.

The physical cross section should be independent of the scale: the dependence in eq. (8) introduces an unphysical parameter. If the perturbative expansion is convergent, *i.e.* if further higher-order corrections are small, at some scale the $\mathcal{O}(\alpha_s^{n+1})$ contribution to the cross section should be smaller than the $\mathcal{O}(\alpha_s^n)$ contribution³. If the scale dependence is strong, the perturbative expansion is untrustworthy [11]. Since $K_{\text{th}} - 1 > 1$, further higher-order corrections are needed, particularly for charm and bottom quarks which are rather “light” when \sqrt{S} is large. Although the scales are, in principle, independent, we take $\mu_F = \mu_R = \mu$ unless otherwise noted because this assumption is inherent in global analyses of parton densities. Sometimes we use the notation $\mu = \sqrt{Q^2}$.

The two loop value of the strong coupling constant, α_s , depends on the number of active flavors, f , and the appropriate value of Λ_{QCD} for the number of flavors, Λ_f ,

$$\alpha_s(\mu, f) = \frac{1}{b_f \ln(\mu^2/\Lambda_f^2)} \left[1 - \frac{b'_f \ln \ln(\mu^2/\Lambda_f^2)}{b_f \ln(\mu^2/\Lambda_f^2)} \right], \quad (9)$$

where $b_f = (33 - 2f)/12\pi$ and $b'_f = (153 - 19f)/(2\pi(33 - 2f))$. For charm and bottom production, $f = 3$ and 4. Parton densities are calculated assuming the heavy quark contributions turn on at $\mu = m_Q$ and $\alpha_s(m_Q, f) = \alpha_s(m_Q, f + 1)$. Above this threshold, some groups, *e.g.* [14], treat the heavy quark as massless in the evolution of the parton densities, introducing some overcounting into production calculations. Also note that the heavy quark

³The order of the expansion is represented by n where $n \geq 2$ for $Q\bar{Q}$ production. A calculation to order $\mathcal{O}(\alpha_s^n)$ introduces corrections at the order $\mathcal{O}(\alpha_s^{n+1})$. Thus the μ dependence should decrease when additional higher-order corrections are included if the perturbation theory converges.

mass threshold chosen in the global analysis of parton densities may differ from the mass used in calculations.

We have used two sets of recent parton distribution functions⁴, GRV HO [16] and MRS D-′ [14]. GRV HO has a low initial scale, $Q_{0,\text{GRV}}^2 = 0.3 \text{ GeV}^2$, with valence-like parton distributions, therefore evolving very quickly with Q^2 . MRS D-′ has a more conventional initial scale, $Q_{0,\text{MRS}}^2 = 5 \text{ GeV}^2$, and sea quark and gluon densities that grow as $\sim x^{-1/2}$ when $x \rightarrow 0$. The difference in Q_0^2 produces the contrast in $Q\bar{Q}$ production between the two sets. Both are compatible with the recent deep-inelastic scattering data from HERA [17] although both are on the high side of the data. We also use the SMRS P2 [18] and GRV HO pion [19] densities. The GRV HO pion distributions are obtained from their proton set and have a similar behavior at low x . The SMRS P2 distributions are based on an older set of nucleon distributions with a different value of Λ_4 than MRS D-′. In this case, we evaluate α_s at the MRS D-′ value of Λ_4 . Also, note that at $Q_{0,\text{MRS}}^2$, the pion sea quark and gluon distributions are assumed to be constant as $x \rightarrow 0$, incompatible with the MRS D-′ low x behavior.

Since we will discuss both $p(\bar{p})p$ and π^-p production, it is instructive to show the quark and gluon momentum distributions for protons and pions. In Fig. 2(a) and (c) we show $xf(x) = x(u_V(x) + d_V(x) + 2(\bar{u}(x) + \bar{d}(x) + \bar{s}(x))) = x(u_V(x) + d_V(x) + S(x))$ and $xg(x)$ at $Q^2 = 5, 25, \text{ and } 100 \text{ GeV}^2$. The lower curve for each set corresponds to the lowest Q^2 , typical for charm production. The middle curve, at 25 GeV^2 , represents charm production at $p_T \simeq 3.5m_c$ and b production at $\mu \simeq m_b$. The highest Q^2 is equivalent to c and b production at $p_T > m_Q$. In 2(b) and (d), we show the parton distributions as a function of Q^2 for $x = 0.0025, 0.007, \text{ and } 0.15$. Here the lowest x values correspond to b production at CDF and UA1. We choose $x = 0.15$ as typical of central charm production at fixed target

⁴All available parton distribution functions are contained in the package PDFLIB [15], available in the CERN library routines.

energies. The curves are MRS D-′ (solid), GRV HO (dashed), SMRS P2 (dot-dashed), and GRV HO pion (dotted). At fixed Q^2 , parton distributions that initially increase as $x \rightarrow 0$ are depleted at higher x compared to constant initial distributions such as SMRS P2. The pion quark distributions are larger than the proton distributions as $x \rightarrow 1$. When the partonic cross sections are convoluted with the parton densities, gg and qg processes dominate because the flux, $\propto F_i^A(x_1, \mu_F)F_j^B(x_2, \mu_F)^5$, is large. In fact, although the gluon density is larger at small x , as x increases, it drops faster than the quark density so that, at some x_1x_2 , $F_q^A F_g^B > F_g^A F_q^B$. Eventually, as $x_1x_2 \rightarrow 1$, $q\bar{q}$ annihilation dominates since the valence quark density is most important at large x .

In Fig. 3(a), we show the scale dependence of the NLO calculations with the pp and pA data on $\sigma_{c\bar{c}}^{\text{tot}}(S)$ [4,5,20] assuming a linear nuclear dependence [21]. The scale is varied between $m_Q/2$ and $2m_Q$ with $1.2 < m_Q < 1.8$ GeV to show the range of theoretical uncertainty [6,20]. We further assumed that $\sigma(D_s) \approx 0.2\sigma(D^0 + D^+)$ and $\sigma(\Lambda_c) \simeq 0.3\sigma(D^0 + D^+)$ so that $\sigma_{c\bar{c}}^{\text{tot}} \approx 1.5\sigma(D\bar{D})$, as in Ref. [20]. Since $m_c < Q_{0,\text{MRS}}$, we take $\mu_F = 2m_c$ for the calculations with the MRS parton densities. The three solid curves are calculated with MRS D-′ densities and $m_c = 1.2$ GeV, $\mu_R = m_c/2$ (upper); $m_c = 1.2$ GeV, $\mu_R = 2m_c$ (middle); and $m_c = 1.8$ GeV, $\mu_R = 2m_c$ (lower). The difference between the upper and lower curves gives the maximum variation of $\sigma_{c\bar{c}}^{\text{tot}}$ for these densities, a factor of 90 for $\sqrt{S} = 20$ GeV and 20 for $\sqrt{S} = 14$ TeV. If the MRS D0′ set is used at the same mass and scale, the cross section is slightly larger at fixed-target energies because the D0′ gluon density is larger for $x > 0.06$ but since $xg(x \rightarrow 0, Q_{0,\text{MRS}}^2) \rightarrow \text{constant}$, $\sigma_{c\bar{c}}^{\text{tot}}(\text{D-}')/\sigma_{c\bar{c}}^{\text{tot}}(\text{D0}') \approx 20$ at 14 TeV. The corresponding K factors are given by the solid line in Fig. 3(b)— K_{th} has very little scale dependence with these parton densities.

Because the GRV HO distributions have a much lower Q_0 , we take $\mu_R = \mu_F$. The dot-dashed and dotted curves show $\mu = m_c/2$ and $\mu = 2m_c$. The upper curves have $m_c = 1.2$

⁵In this notation, *e.g.* $F_g(x) = g(x)$.

GeV, the lower, $m_c = 1.8$ GeV. Even though the cross section is larger at low \sqrt{S} for $\mu = m_c/2$, as the energy increases, the small x gluon density at the higher scale becomes the dominant feature, causing the crossover shown at high energy. In fact, because the gluon density starts out valence-like at $Q_{0,\text{GRV}}$, it is almost constant for x values probed at $\sqrt{S} > 100$ GeV for $\mu = 0.6$ GeV, causing the sudden flattening of the upper dot-dashed curve. The variation in K_{th} is large when $\mu = m_c/2$. When $\mu = 2m_c$, K_{th} is approximately the same as the MRS distributions. However, the maximum variation of $\sigma_{c\bar{c}}^{\text{tot}}$ is smaller for the GRV HO densities, a factor of 60 for $\sqrt{S} = 20$ GeV and 6 for $\sqrt{S} = 14$ TeV (excluding $\mu = 0.6$ GeV).

Previously [9], the NLO calculations were compared to the data to fix m_c and μ at $K_{\text{exp}}^{\text{NLO}} \sim 1$ to provide an estimate that could be extrapolated to nuclear collider energies. Reasonable agreement was found for $m_c = 1.2$ GeV, $\mu = 2m_c$ for MRS D- $'$ (central solid curve) and $m_c = 1.3$ GeV, $\mu = m_c$ for GRV HO (dashed curve)⁶. Note however that both curves tend to underestimate $\sigma_{c\bar{c}}^{\text{tot}}$ with $K_{\text{exp}}^{\text{NLO}} \sim 1.1 - 2$. In the range of the parameter space defined by m_Q , μ_R and μ_F , $K_{\text{exp}}^{\text{NLO}}$ can be reduced to unity. However, it is questionable if the mass and scale values needed for $K_{\text{exp}}^{\text{NLO}} \sim 1$ are consistent with a perturbative treatment and with the defined limits of the parton density distributions⁷. It is also not clear that the NNLO corrections to heavy quark production would not be at least as large as the NLO corrections, particularly when $m_Q \ll \sqrt{S}$, even though for high-mass Drell-Yan production

⁶A comparison to the $c\bar{c}$ data with π^- beams [4,5,20] using the same parameters gives agreement with the data at a similar level.

⁷Recently, $m_c = 1.5$ GeV was found to be compatible with this data with some essential caveats: μ_F and μ_R were varied independently and out-of-date parton distributions fit with several values of Λ_{QCD} were used [20]. Decreasing μ_R with respect to μ_F and increasing Λ_{QCD} result in significantly larger cross sections for a given m_c . Additionally, different parton densities were used in the calculations of $\sigma_{Q\bar{Q}}^{\text{tot}}$ and high energy b production.

at NNLO $\sigma_{\text{NNLO}}/\sigma_{\text{NLO}} \sim 1.1\text{-}1.3$ [22], due to cancellations among the different channels.

However, the variation in $\sigma_{b\bar{b}}^{\text{tot}}$ is much smaller than $\sigma_{c\bar{c}}^{\text{tot}}$. For $\mu = m_b$, $\sigma(m_b = 4.5 \text{ GeV})/\sigma(m_b = 5 \text{ GeV}) \approx 25$ at $\sqrt{S} = 40 \text{ GeV}$ and 1.4 for 14 TeV while for $m_b = 4.75 \text{ GeV}$, $\sigma(\mu_b = 0.5m_b)/\sigma(\mu_b = 2m_b) \approx 3$ at $\sqrt{S} = 40 \text{ GeV}$ and 1.2 at 14 TeV. The K factor is also smaller; $K_{\text{th}} \approx 1.2 - 2.5$.

In Fig. 4 we show the scale variation of $\sigma_{c\bar{c}}^{\text{tot}}$ for π^-p production at 340 GeV (a) and pp production at 800 GeV (b) using the GRV HO pion and nucleon distributions. As μ/m_c increases at fixed energy, the cross section varies less rapidly but K_{th} increases for $\mu > m_c$. There is no value of μ where the NLO corrections to the Born cross section are minimal, *i.e.* no optimal scale [23].

Although there is no physical reason for assuming that μ_F and μ_R are different because they are not separated in analyses of the parton densities, we also show the change of the $c\bar{c}$ cross section in π^-p production with $p_\pi = 500 \text{ GeV}$ induced by varying the scales independently: $\mu_F = m_c$ in 4(c) and $\mu_R = m_c$ in 4(d). In addition to the GRV HO results, we include the calculations with the MRS D-' parton distributions and $\mu_F = 2m_c$ in (c) and $\mu_R = 2m_c$ in (d) at NLO (dot-dashed) and the Born level (dotted). The running of α_s is the source of the strong dependence observed in (c). When $\mu_R < m_c$, the coefficients \bar{f}_{ij}^1 , usually negative, produce an overall enhancement of $\hat{\sigma}_{ij}$. However for $\mu_R > m_c$, the variation of $\hat{\sigma}_{ij}$ with μ decreases since the NLO corrections partially cancel each other. There is no strong effect on K_{th} . In (d), the increase in $\sigma_{c\bar{c}}^{\text{tot}}$ for $\mu_F < m_c$ with the GRV HO distributions occurs because at $\mu_F \approx Q_{0,\text{GRV}}$ and low x , the sea quark and gluon distributions are valence-like [16]. The MRS D-' variation is negligible since $\mu_F < Q_{0,\text{MRS}}$ for $\mu_F/m_c < 2.7$, thus $\mu_F \equiv Q_{0,\text{MRS}}$.

Until now, we have discussed $\sigma_{Q\bar{Q}}^{\text{tot}}$ where $\mu \propto m_Q$. However, for single inclusive or double differential distributions, it may be more appropriate to choose a scale proportional to the transverse momentum of the heavy quark, p_T , or its transverse mass, m_T . The transverse momentum is a natural scale in jet and prompt photon production with massless final-state

particles. Additionally, since $p_T, m_T \propto (t - m_Q^2)(u - m_Q^2)/s \rightarrow (T - m_Q^2)(U - m_Q^2)/S$, this choice is invariant under scale transformations of the initial state momenta and results in a simple relation between the partonic and hadronic variables, unlike the choice $\mu = s$. A constant scale would be appropriate if $m_Q \simeq p_T$, but generally $m_c \ll p_T$ and $m_b \ll p_T$ at collider energies. Therefore the p_T dependent scale absorbs (resums) large logarithmic terms such as $\ln(p_T/m_Q)$ appearing when $p_T \gg m_Q$ and producing collinear divergences [7] which are unregulated if $\mu = m_Q$. We examine the p_T distributions of b quark production at collider energies for two specific cases, a constant scale, $\mu \propto m_b$, and running scale, $\mu \propto m_T$, to see if the data favors a particular scale. We also show the p_T distributions and $K_{\text{th}}(p_T)$ for charmed quarks at fixed target energies.

We first compare the constant and running scales for single b production from the $p\bar{p}$ colliders at $\sqrt{S} = 630$ GeV and 1.8 TeV. The measurements are integrated over p_T above each $p_{T,\text{min}}$. We use $m_b = 4.75$ GeV. The NLO calculations with the GRV HO distributions are shown in Fig. 5(a) for UA1 [24] and Fig. 5(b) for CDF [25] and D0 [26]. The solid curves show $\mu = m_T$, the dashed curves, $\mu = m_b$. Neither are clearly favored by the data. The Tevatron data is also compared to calculations with $\mu = m_T/4$ and $m_b/4$. However $\mu = m_b/4$ is in clear contradiction with the data.

In Fig. 6(a) we show the charmed quark p_T distributions for π^-p production with $p_{\text{lab}} = 500$ GeV using the GRV HO distributions. The solid and dashed curves are the NLO and Born results for $\mu = m_T$ while the dot-dashed and dotted curves are the calculations with $\mu = m_c$. The NLO result drops below the Born for $p_T > 4$ GeV. High statistics charm measurements should be able to detect a decrease in the slope of the p_T distribution for $p_T > 4$ GeV if nature favors the constant scale. No such change has been observed at present although data in this region is rather scarce. The resulting ratios $K_{\text{th}}(p_T)$ are shown in Fig. 6(b) for the running scale (solid curve) and the fixed scale (dashed curve). When the scale increases with p_T , K_{th} is relatively constant or decreases slightly. However, the fixed scale produces a strong decrease of K_{th} with p_T .

The calculations in Fig. 6(a) and (b) are particularly illustrative of both how the pro-

duction processes compete with each other and the relative importance of the NLO corrections for each process. The crossover of the Born and NLO p_T distributions with the fixed scale, occurring at $p_T \approx 4$ GeV, can be understood by an examination of the coefficients of the perturbative expansion. To schematically illustrate the p_T dependence, we can take $1/\sqrt{\rho} \approx \sqrt{s}/2m_T$ in Fig. 1. In the region $0 < p_T < 5$ GeV, $1/\sqrt{\rho} < 12$. For $1/\sqrt{\rho} \leq 4$, $f_{gg}^0 > f_{gg}^1$ while f_{gg}^1 dominates for $1/\sqrt{\rho} \geq 4$. Both coefficients are always positive although \bar{f}_{gg}^1 is negative for $1/\sqrt{\rho} > 2.2$. The coefficient f_{qg}^1 is positive when $1/\sqrt{\rho} > 2.2$ although smaller than f_{gg}^1 ; \bar{f}_{qg}^1 is negative and $f_{qg}^1 > |\bar{f}_{qg}^1|$ for most values of $1/\sqrt{\rho}$. The NLO correction to $q\bar{q}$ annihilation, $f_{q\bar{q}}^1$, is negative for $1.4 < 1/\sqrt{\rho} < 4.5$. When $\mu \neq m_Q$, $\bar{f}_{q\bar{q}}^1$ can partially compensate for this negative contribution. As p_T increases, $1/\sqrt{\rho}$ enters the region of negative $f_{q\bar{q}}^1$ at $p_T \approx 4$ GeV while $f_{q\bar{q}}^0$ is large and positive. At the same time the Born contribution to gg fusion becomes larger than the NLO correction. These competing terms produce the crossover observed in Fig. 6(a) for the constant scale. The same effect causes the turnover in the dashed curve of Fig. 5(a) for $p_{T,\min} \approx 50$ GeV. Thus the constant scale, although introducing divergences, shows the structure of the NLO corrections.

Assuming that $\mu \propto m_T$ softens these effects, partially because of the \bar{f}_{ij}^1 contributions but mainly due to the evolution of the parton densities. As p_T increases, x_1 and x_2 also increase so that while the Q^2 evolution increases the parton density at fixed x , the higher x values actually deplete the parton flux. This relative balance produces a nearly constant K_{th} . Results with the MRS distributions are shown in Fig. 6(c) and (d). Since $\mu = 2m_c$ for the fixed scale, a larger p_T is needed to enter the crossover region in $1/\sqrt{\rho}$.

We now turn to the scale dependence of heavy quark distributions at nuclear collider energies. While the NLO calculations are needed for the p_T dependence of $Q\bar{Q}$ pair production and decay, trivial at the Born level, it would be convenient if the other relevant distributions could be modeled by the Born distributions to within a constant K factor. The $Q\bar{Q}$ pair distributions are essential to determine the heavy quark contribution to lepton pair production. In Figs. 7-10 we show K_{th} for $\sqrt{s} = 200$ GeV (RHIC) and 5.5 TeV (LHC) for c and b production assuming $\mu = m_T$ for single inclusive quark x_F , rapidity, and p_T^2 distributions in

(a), (c), and (e) respectively. The $Q\bar{Q}$ pair x_F , y , and invariant mass distributions are shown in (b), (d), and (f). For the pair distributions, we assume $\mu \propto \sqrt{m_Q^2 + (p_{T,Q}^2 + p_{T,\bar{Q}}^2)/2}$. The results with the GRV HO parton densities are given by the circles while the diamonds are the MRS D-’ results. (For the NLO distributions themselves, see Ref. [9].) With the running scale, K_{th} is indeed nearly constant for these quantities, even in a regime where $m_Q \ll \sqrt{S}$. Some variations occur near the boundaries of phase space, seen in the c and b quark rapidity distributions at $\sqrt{S} = 200$ GeV. The K factors are independent of parton density except for charm production at $\sqrt{S} = 5.5$ TeV where K_{th} is larger for the GRV HO distributions. For the charmed quark, $K_{\text{th}}(p_T^2)$ increases 50% at $\sqrt{S} = 200$ GeV and a factor of two at $\sqrt{S} = 5.5$ TeV. These increases perhaps indicate the appearance of large logarithms that need to be resummed in the p_T distributions. Although some variation appears, event generators for heavy quark production can, with relative confidence, scale all non-trivial Born results⁸.

Thus for heavy quark and quark pair distributions calculable at the Born level, K_{th} is nearly constant provided that $\mu \propto m_T$. The actual value of K_{th} can be determined by a comparison of the NLO and Born total cross sections. We have set the scale by making $K_{\text{exp}}^{\text{NLO}}$ close to unity to better estimate production at nuclear colliders. Other, more sophisticated methods can be used to optimize the scale [23] or relate it to other scales in perturbative QCD [28]. Further theoretical advances can perhaps also reduce the uncertainties. A resummation of the soft gluon contribution to top production near threshold has been performed [29]. This near-threshold resummation may also be applied to charm and bottom [30] production at fixed-target energies, suggesting a more appropriate scale.

⁸A constant scale is assumed in [27], leading to the conclusion that $K_{\text{th}}(p_T)$ is a strongly increasing function of p_T . Our calculations with the constant scale confirm these results in the p_T region explored in [27]. However, we note that for $p_T > 6\text{-}8$ GeV at RHIC K_{th} decreases again while at the LHC K_{th} reaches a plateau when $p_T \sim 10$ GeV.

An understanding of heavy quark production is essential to correctly interpret data from RHIC and the LHC. At these nuclear colliders, $Q\bar{Q}$ production is in the high-energy limit where large logarithmic corrections to $\hat{\sigma}_{ij}(\rho)$ are important. A first attempt has been made to resum the small x corrections to the heavy quark production cross section in the $\rho \rightarrow 0$ regime [31] which could lead to an improvement in the RHIC and LHC estimates.

We thank J.A. Appel, S. Gavin, B.W. Harris, P. Karchin, I. Sarcevic, and J. Smith for stimulating discussions and M.L. Mangano for help with the program package. We also thank the BNL theory group for hospitality during part of this work.

REFERENCES

- [1] R. Vogt, B.V. Jacak, P.L. McGaughey and P.V. Ruuskanen, Phys. Rev. **D49** (1994) 3345.
- [2] A. Shor, Phys. Lett. **B215** (1988) 375. A. Shor, Phys. Lett. **B233** (1989) 231.
- [3] E. Shuryak, Phys. Rev. Lett. **68** (1992) 3270.
- [4] S.P.K. Tavernier, Rep. Prog. Phys. **50** (1987) 1439. This review contains references to all data prior to 1988, including the ISR measurements.
- [5] J.A. Appel, Ann. Rev. Nucl. Part. Science **42** (1992) 367.
- [6] P. Nason, S. Dawson, and R.K. Ellis, Nucl. Phys. **B303** (1988) 607.
- [7] P. Nason, S. Dawson, and R.K. Ellis, Nucl. Phys. **B327** (1989) 49.
- [8] W. Beenakker, H. Kuijf, W.L. van Neerven, and J. Smith, Phys. Rev. **D40** (1989) 54; W. Beenakker, W.L. van Neerven, R. Meng, G.A. Schuler, and J. Smith, Nucl. Phys. **B351** (1991) 507.
- [9] P.L. McGaughey *et al.*, Int. J. Mod. Phys. **A10** (1995) 2999.
- [10] M.L. Mangano, P. Nason, and G. Ridolfi, Nucl. Phys. **B373** (1992) 295. M.L. Mangano, P. Nason, and G. Ridolfi, Nucl. Phys. **B405** (1993) 507.
- [11] R.K. Ellis, in *Physics at the 100 GeV Scale*, Proceedings of the 17th SLAC Summer Institute, Stanford, California, 1989, edited by E.C. Brennan (SLAC Report No. 361, Stanford, 1990).
- [12] J. Smith and W.K. Tung, in *Proceedings of the Workshop on B Physics at Hadron Colliders*, Snowmass, CO, 1993, edited by P. McBride and C.S. Mishra.
- [13] R. Meng, G.A. Schuler, J. Smith, and W.L. van Neerven, Nucl. Phys. **B339** (1990) 325.
- [14] A.D. Martin, W.J. Stirling, and R.G. Roberts, Phys. Lett. **B306** (1993) 145.

- [15] H. Plochow-Besch, *Comp. Phys. Comm.* **75** (1993) 396.
- [16] M. Glück, E. Reya, and A. Vogt, *Z. Phys.* **C53** (1992) 127.
- [17] M. Derrick *et al.*, ZEUS Collaboration, *Phys. Lett.* **B316** (1993) 515.
- [18] P.J. Sutton, A.D. Martin, R.G. Roberts, and W.J. Stirling, *Phys. Rev.* **D45** (1992) 2349.
- [19] M. Glück, E. Reya, and A. Vogt, *Z. Phys.* **C53** (1992) 651.
- [20] S. Frixione, M.L. Mangano, P. Nason, and G. Ridolfi, *Nucl. Phys.* **B431** (1994) 453.
References for total charm cross section data since 1988 can be found here.
- [21] G.Alves *et al.*, E769 Collaboration, *Phys. Rev. Lett.* **70** (1993) 722.
- [22] R. Hamberg, W.L. van Neerven, T. Matsuura, *Nucl. Phys.* **B359** (1991) 343; W.L. van Neerven and E.B. Zijlstra, *Nucl. Phys.* **B382** (1992) 11.
- [23] P.M. Stevenson, *Phys. Rev.* **D23** (1981) 70; P.M. Stevenson and H.D. Politzer, *Nucl. Phys.* **B277** (1986) 758.
- [24] C. Albajar *et al.*, UA1 Collaboration, *Phys. Lett.* **B256** (1991) 121.
- [25] F. Abe *et al.*, CDF Collaboration, Fermilab-Conf-94/134-E; Fermilab-Conf-94/136-E; Fermilab-Conf-94/141-E.
- [26] K. Bazizi, D0 Collaboration, to appear in the *Proceedings of the XXIX Rencontres de Moriond*, Méribel, France, March 1994.
- [27] I. Sarcevic and P. Valerio, *Phys. Lett.* **B338** (1994) 426; AZPH-TH/94-20.
- [28] S.J. Brodsky, G.P. Lepage, and P.B. Mackenzie, *Phys. Rev.* **D28** (1983) 228; S.J. Brodsky and H.J. Lu, SLAC-PUB-6481, hep-ph/9405218.
- [29] E. Laenen, J. Smith, and W.L. van Neerven, *Nucl. Phys.* **B369** (1992) 543.

[30] N. Kidonakis and J. Smith, Stony Brook preprint, ITP-SB-95-16.

[31] See *e.g.* J.C. Collins and R.K. Ellis, Nucl. Phys. **B360** (1991) 3.

Figure Captions

Figure 1. The coefficients of the perturbative expansion, $f(\rho)$, given in Ref. [6] and shown as a function of $1/\sqrt{\rho}$. The solid line is the Born contribution, f_{ij}^0 , the dot-dashed and dashed, the NLO corrections f_{ij}^1 and \bar{f}_{ij}^1 for (a) $q\bar{q}$ annihilation, (b) gluon fusion, and (c) quark-gluon scattering.

Figure 2. The parton distributions $x f(x) = x(u_V(x) + d_V(x) + S(x))$ and $x g(x)$ as a function of x and Q^2 . In (a) and (c), $Q^2 = 5, 25,$ and 100 GeV^2 for the lower, middle, and upper curves respectively. In (b) and (d), $x = 0.0025, 0.007,$ and 0.15 in the upper, middle, and lower curves respectively. The curves are MRS D-′ (solid), GRV HO (dashed), SMRS P2 (dot dashed), and GRV HO pion (dotted).

Figure 3. The variation in $\sigma_{c\bar{c}}^{\text{tot}}(S)$ and $K_{\text{th}}(S)$ with parton density, m_c and μ . In (a) the three solid curves are calculated with MRS D-′ densities and $m_c = 1.2 \text{ GeV}, \mu_R = m_c/2$ (upper); $m_c = 1.2 \text{ GeV}, \mu_R = 2m_c$ (middle); and $m_c = 1.8 \text{ GeV}, \mu_R = 2m_c$ (lower). The other calculations are with the GRV HO densities. The dot-dashed and dotted curves show $\mu = m_c/2$ and $\mu = 2m_c$. The upper set has $m_c = 1.2 \text{ GeV}$, the lower, $m_c = 1.8 \text{ GeV}$. The dashed curve is $m_c = 1.3 \text{ GeV}, \mu = m_c$. K_{th} is shown in (b). The solid curve is MRS D-′, $m_c = 1.2 \text{ GeV}, \mu = 2m_c$, the dotted curve GRV HO, $m_c = 1.2 \text{ GeV}, \mu = 2m_c$. The dot-dashed curves are GRV HO, $\mu = 0.5m_c$, and $m_c = 1.2 \text{ GeV}$ (upper), 1.8 GeV (lower).

Figure 4. The variation of $\sigma_{c\bar{c}}^{\text{tot}}$ with $\mu = \mu_F = \mu_R$ for $\pi^- p$ production at 340 GeV (a) and pp production at 800 GeV (b) using GRV HO. The change of the $c\bar{c}$ cross section in $\pi^- p$ production with $p_\pi = 500 \text{ GeV}$ from varying the scales independently is shown for $\mu_F = nm_Q$ in (c) and for $\mu_R = nm_Q$ in (d) where $n = 1$ for GRV HO and 2 for MRS D-′. The curves are GRV HO NLO (solid), Born (dashed), MRS D-′ NLO (dot-dashed), Born (dotted).

Figure 5. Single b production at NLO is compared with data from UA 1 (a) and CDF (b).

The solid curves show $\mu = m_T$ and the dashed curves, $\mu = m_b$. We also present $\mu = m_T/4$ and $m_b/4$ in the upper solid and dashed curves of (b).

Figure 6. The charmed quark p_T distribution for $\pi^- p$ production with $p_{\text{lab}} = 500$ GeV is shown in (a) for the GRV HO parton distributions. The solid and dashed curves are the NLO and Born results for $\mu = m_T$ while the dot dashed and dotted curves are for $\mu = m_c$. In (b) we show the K_{th} factors for the running scale (solid curve) and the fixed scale (dashed curve). The results with MRS D-’ distributions are given in (c) and (d).

Figure 7. The ratios K_{th} for charm production at $\sqrt{S} = 200$ GeV assuming $\mu = m_T$ for single inclusive quark x_F , rapidity, and p_T^2 distributions in (a), (c), and (e) respectively. The $Q\bar{Q}$ pair x_F , y , and invariant mass distributions are shown in (b), (d), and (f). The GRV HO results are given by the circles, MRS D-’, the diamonds.

Figure 8. The same as Fig. 5 for charm production at $\sqrt{S} = 5.5$ TeV.

Figure 9. The same as Fig. 5 for bottom production at $\sqrt{S} = 200$ GeV.

Figure 10. The same as Fig. 5 for bottom production at $\sqrt{S} = 5.5$ TeV.

Figure 1

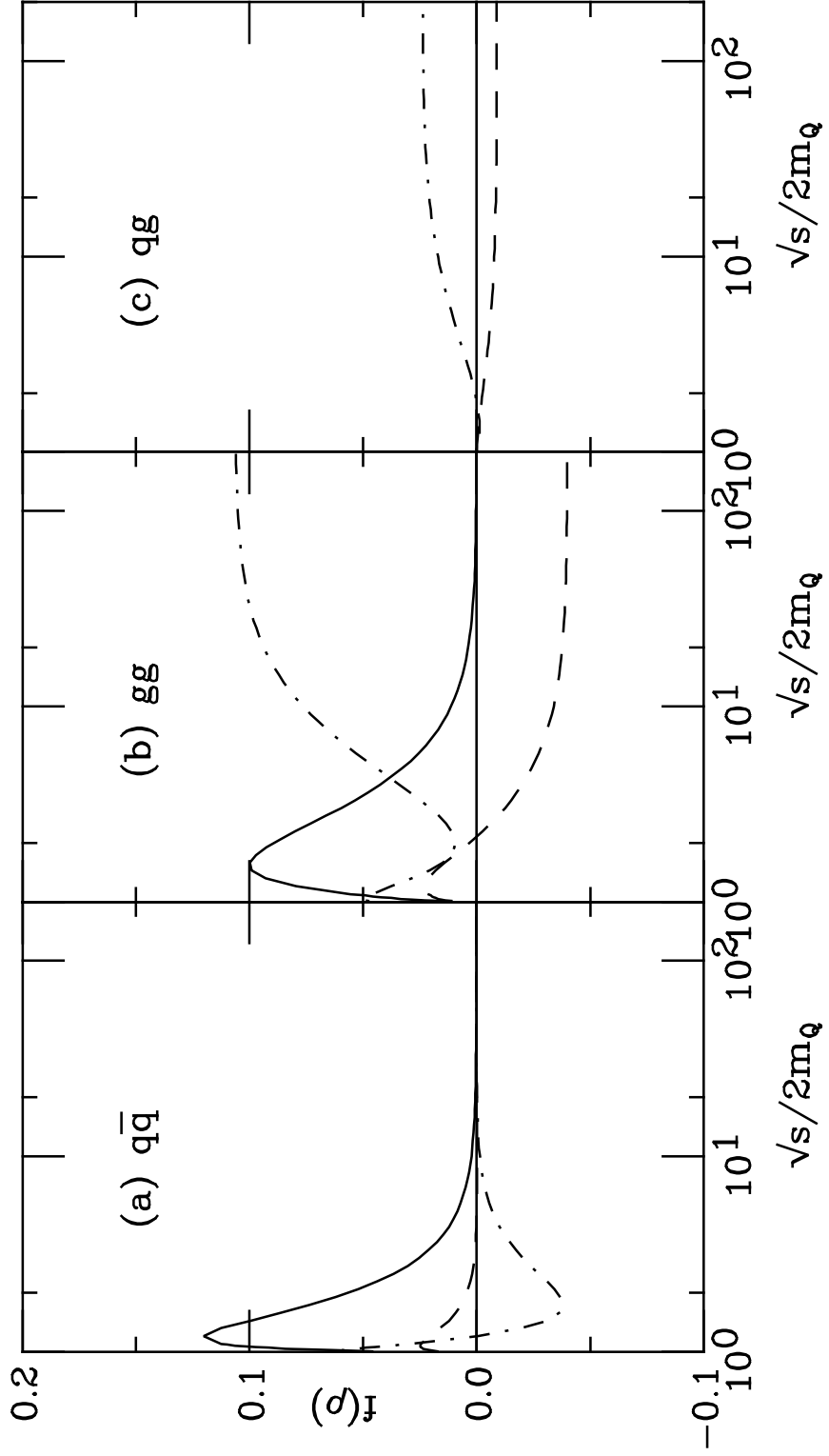


Figure 2

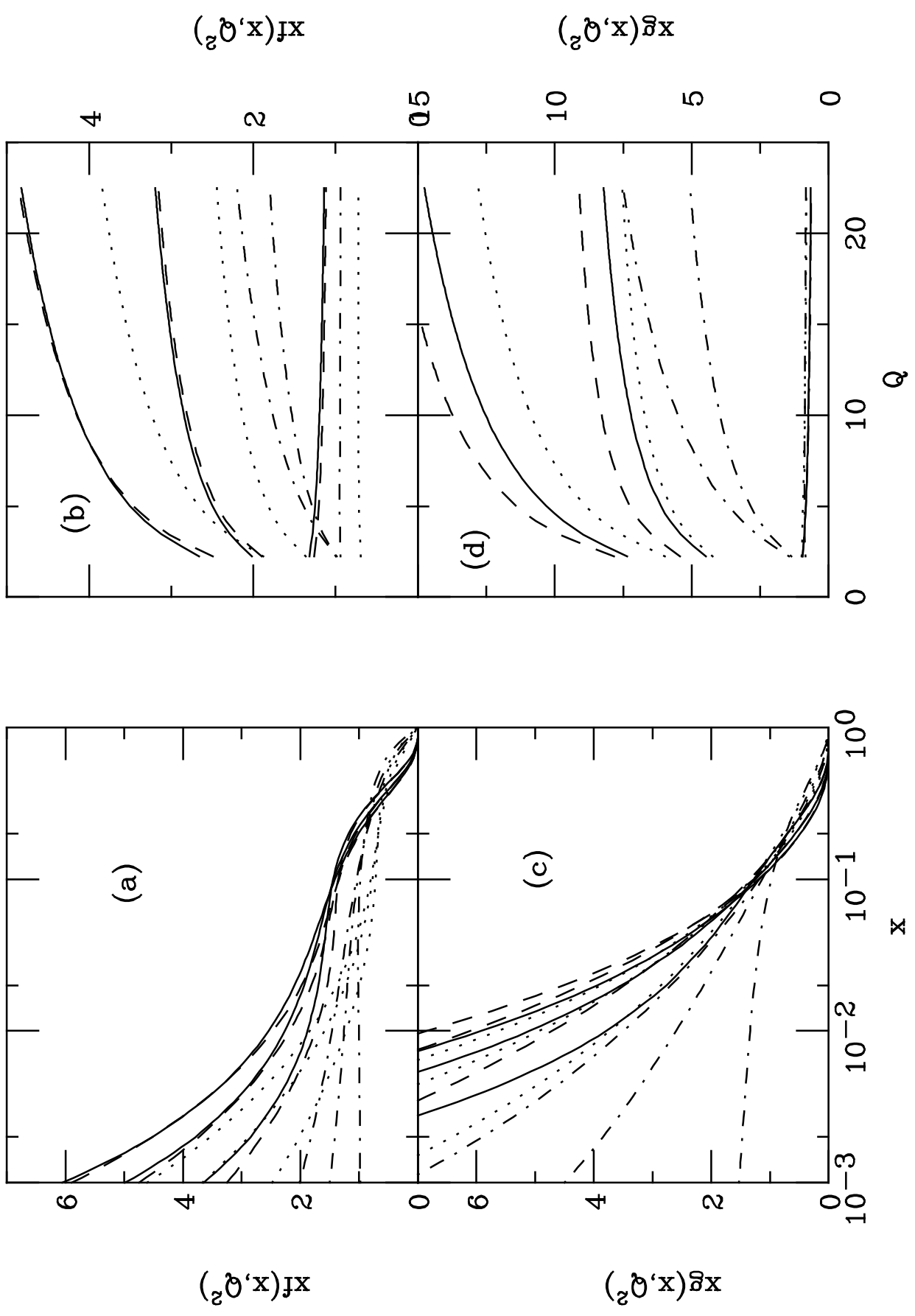


Figure 4

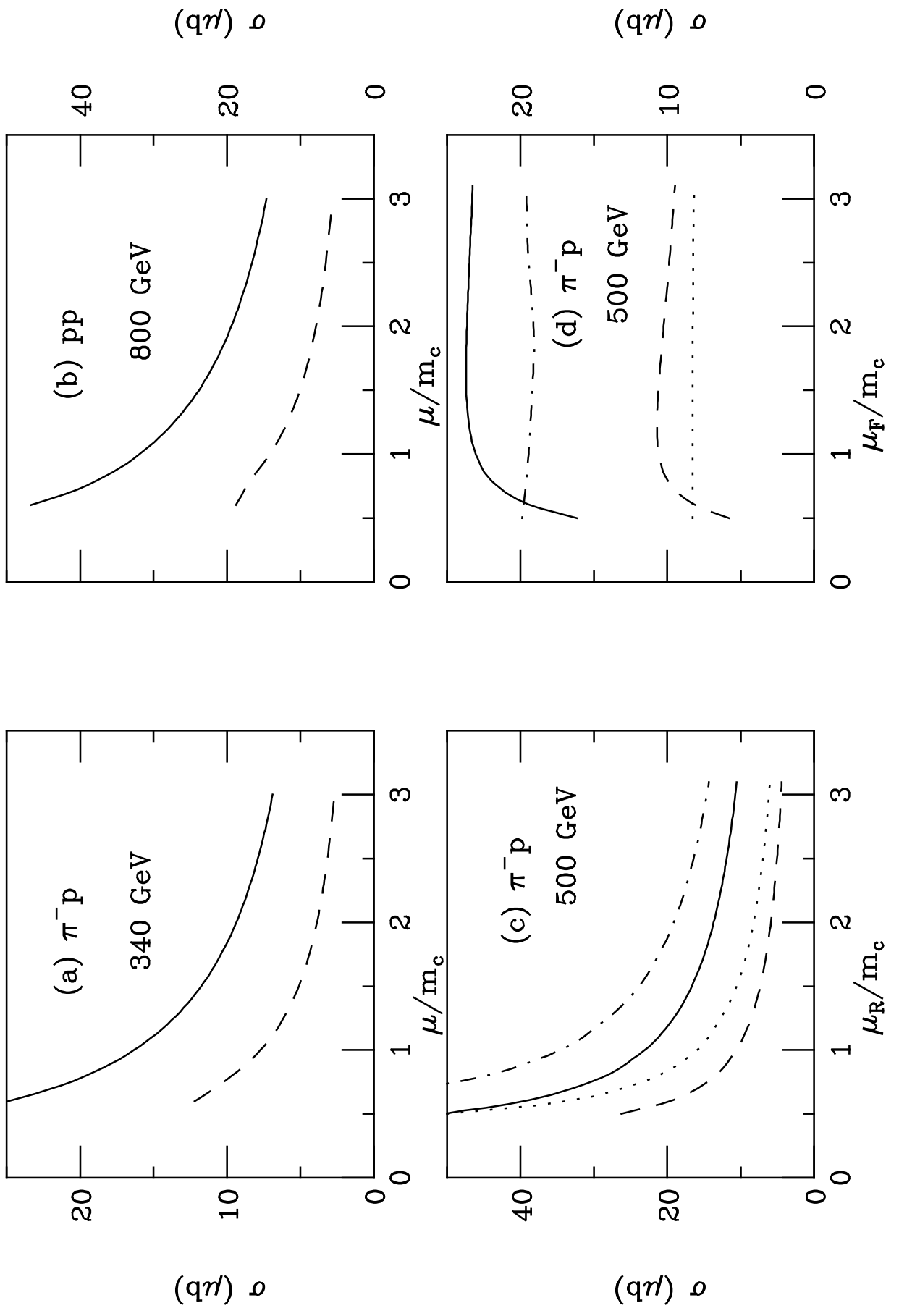


Figure 5

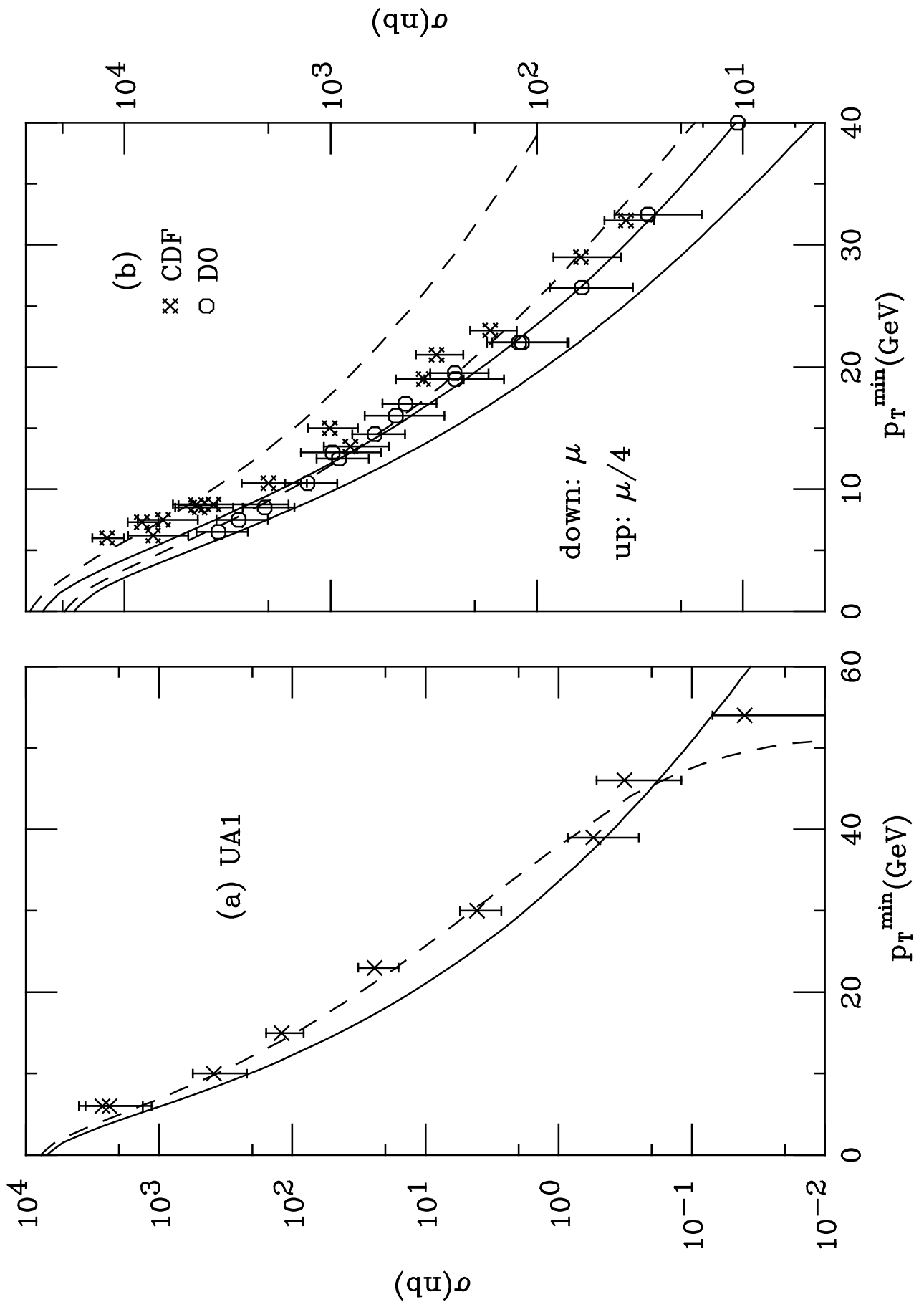


Figure 6

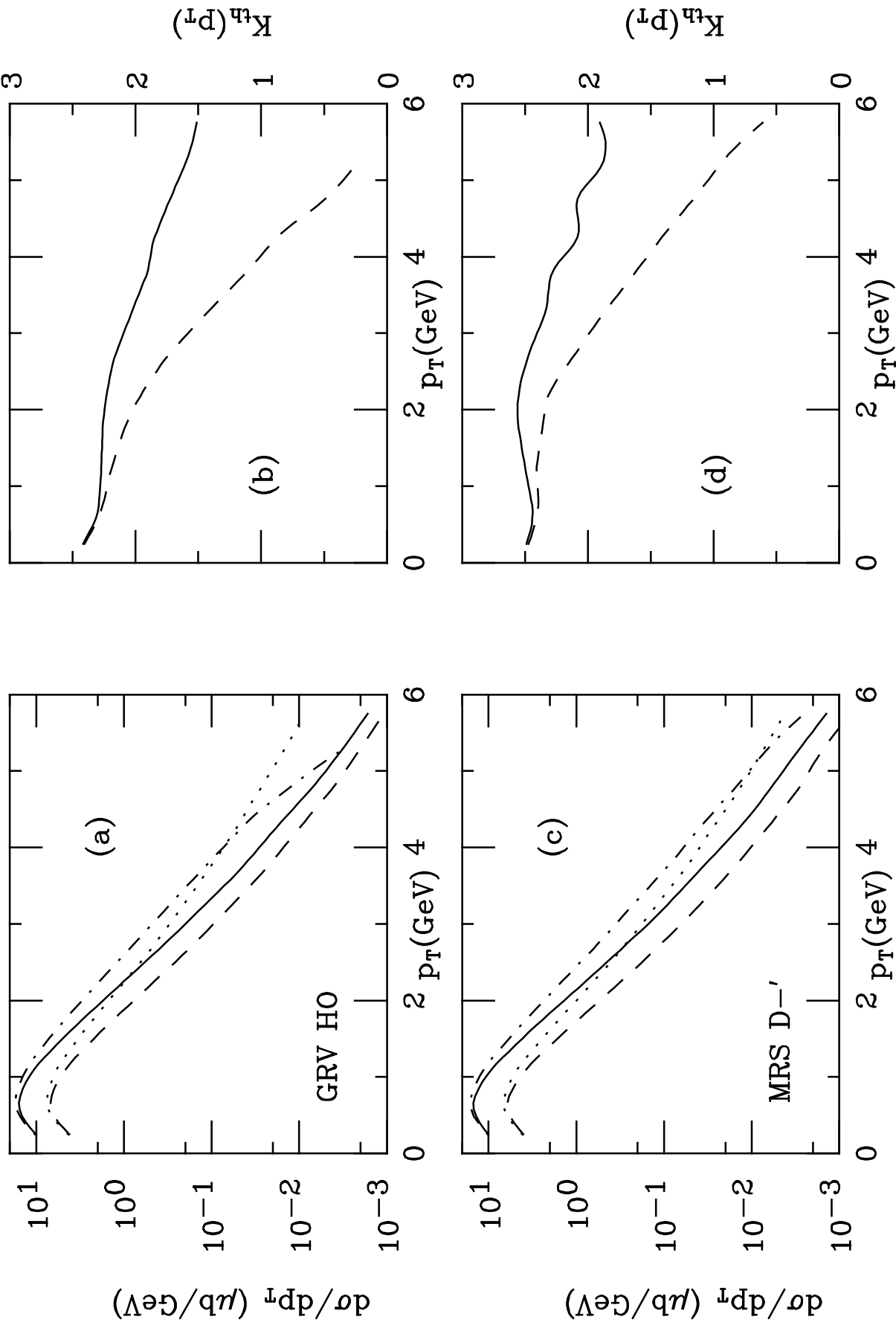


Figure 7

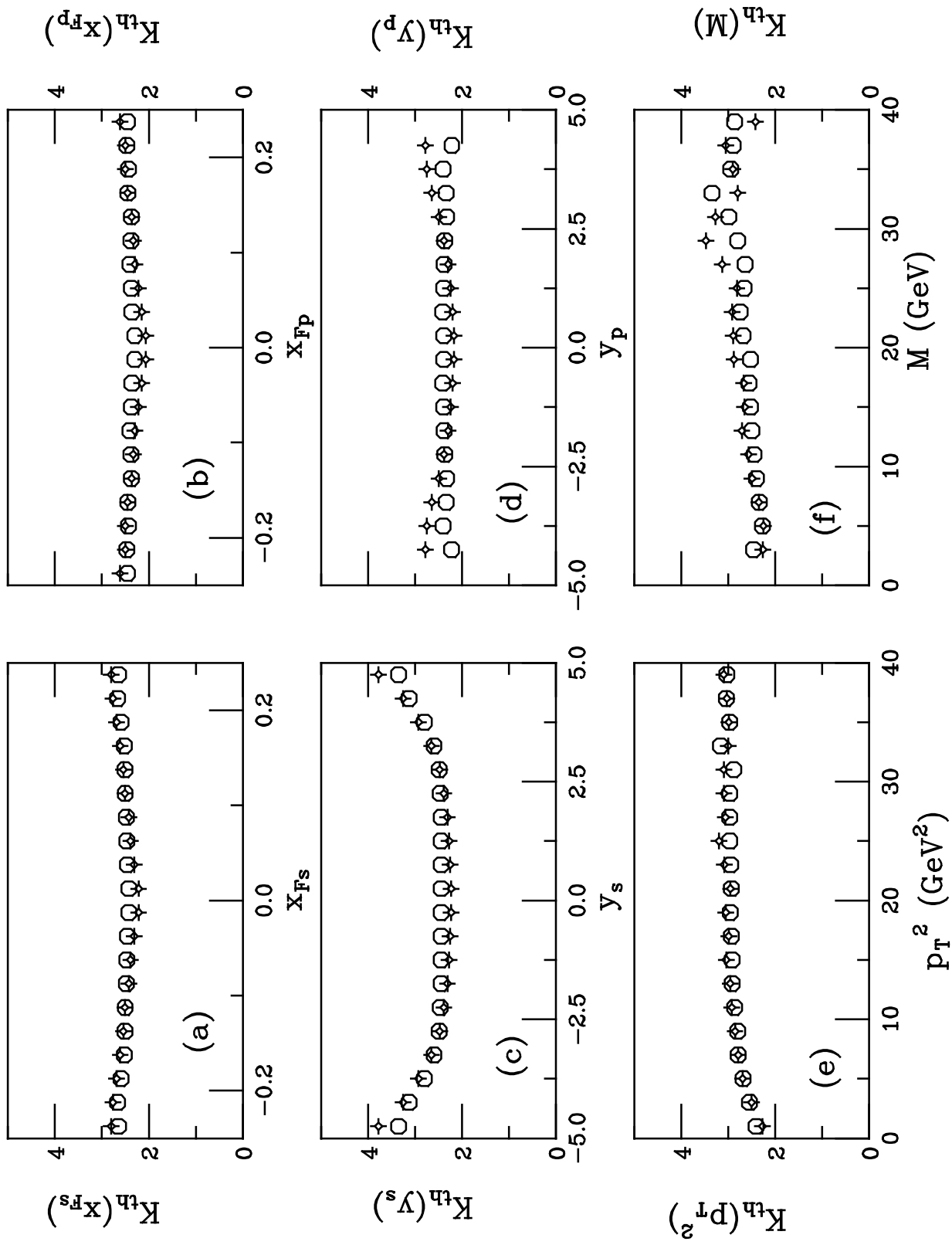


Figure 8

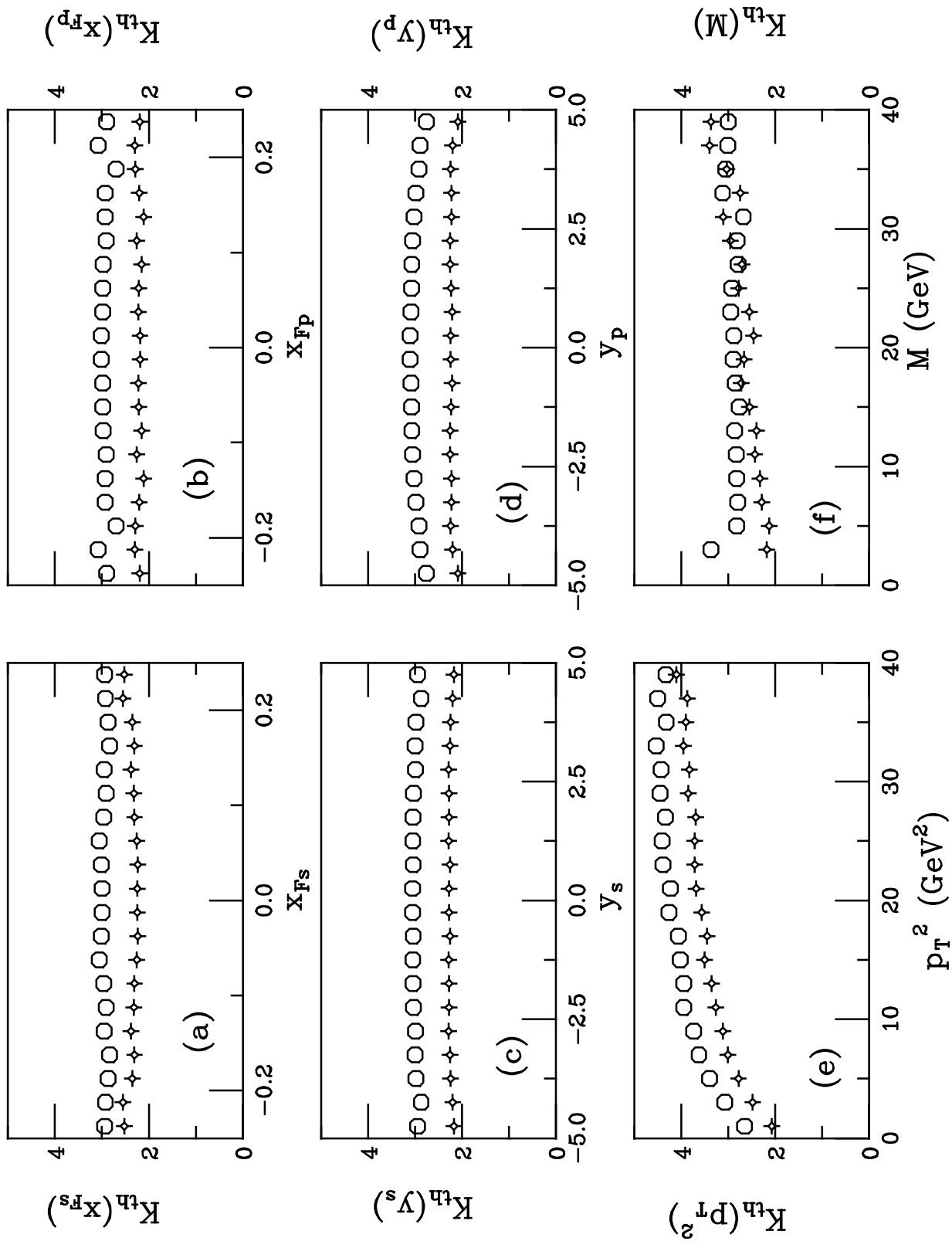


Figure 9

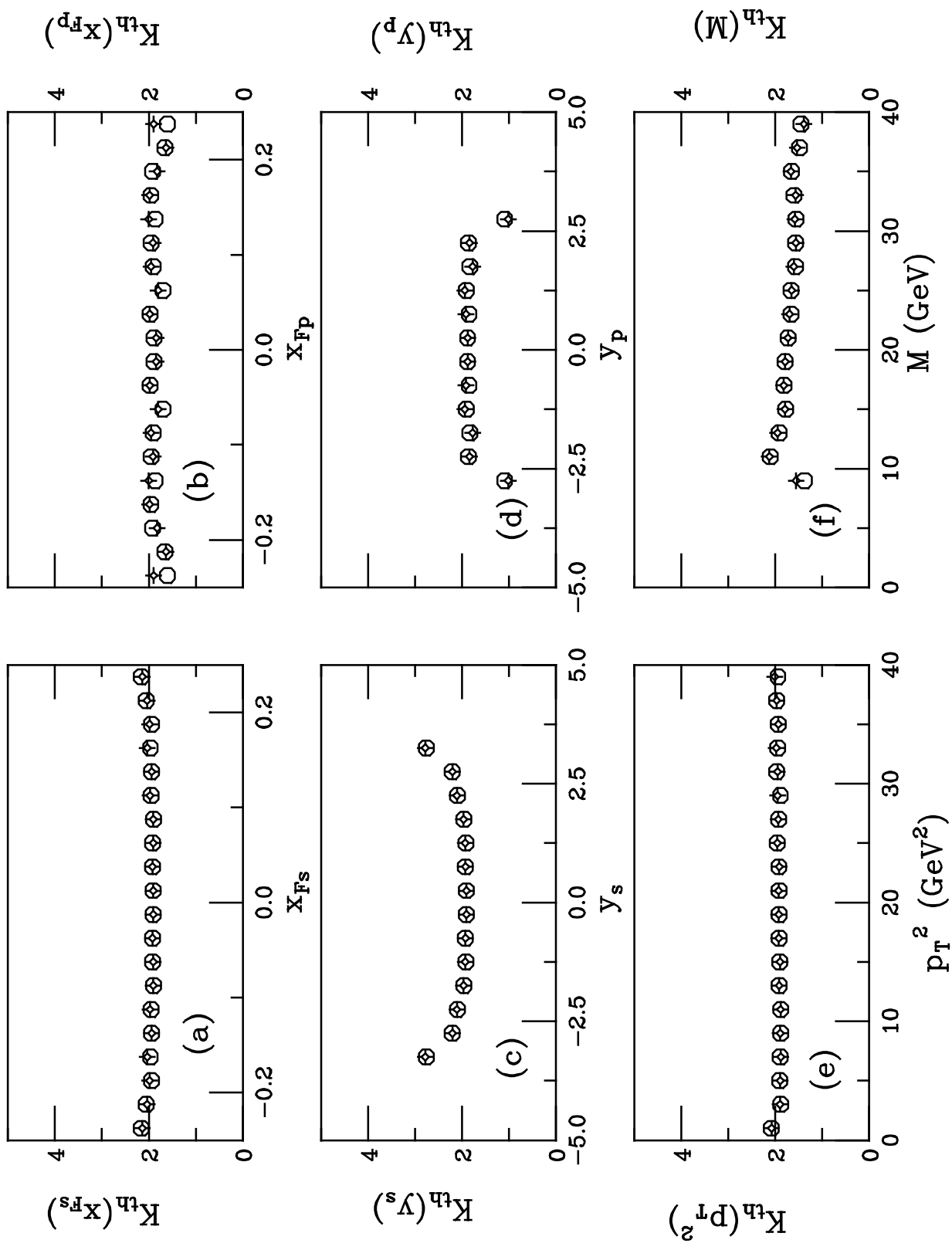


Figure 10

